HHS Public Access

Author manuscript

Oncogene. Author manuscript; available in PMC 2019 December 20.

Published in final edited form as:

Oncogene. 2019 July ; 38(29): 5751–5765. doi:10.1038/s41388-019-0839-x.

SOD1 is essential for oncogene-driven mammary tumor formation but dispensable for normal development and proliferation.

Maria Gomez, **Nagma Shah**, **Timothy C. Kenny**, **Edmund C. Jenkins Jr.**, and **Doris Germain***

Icahn School of Medicine at Mount Sinai, Tisch Cancer Institute, Department of Medicine, division of Hematology/Oncology, New York, New York, USA

Abstract

We previously reported that the dismutase SOD1 is overexpressed in breast cancer. However, whether SOD1 plays an active role in tumor formation *in vivo* has never been demonstrated. Further, as luminal cells of normal breast epithelial cells are enriched in SOD1, whether SOD1 is essential for normal mammary gland development has never been determined. We initiated this study to investigate the role of SOD1 in mammary gland tumorigenesis as well as in normal mammary gland development. We crossed the inducible erbB2 (MMTV-iErbB2) and Wnt (MMTV-Wnt) transgenic mice to the SOD1 heterozygote or knockout mice. Our results show that SOD1 is essential for oncogene-driven proliferation, but not normal proliferation of the mammary gland associated with pregnancy or other normal proliferative tissues such as skin and intestines. We show that activation of the oncogene ErbB2 is associated with increased ROS and that high ROS sub-population of ErbB2 cancer cells show elevated SOD1. In the same cells, decrease in SOD1 is associated with an elevation in both apoptosis as well as oncogene-induced senescence. Based on these results, we suggest that SOD1 carries a housekeeping function that maintains ROS levels below a threshold that supports oncogene-dependent proliferation, while allowing escape from oncogene-induced senescence, independently of the oncogene driving tumor formation. These results identify SOD1 as an ideal target for cancer therapy as SOD1 inhibitors hold the potential to prevent the growth of cancers cells of diverse genotypes, activate multiple modes of cell death therefore making acquired resistance more difficult, while sparing normal tissues.

Keywords

dismutase; SOD; reactive oxygen species; cancer; oncogene-induced senescence

Introduction

Despite the fact that chemotherapy is linked to significant toxicity and morbidity, it remains the main treatment against cancer. The toxicity associated with chemotherapy results from

*Corresponding author, doris.germain@mssm.edu.

Conflict of interest statement: The authors declare that they do not have conflict of interest regarding this study.

its effect on normal proliferation of tissues such as hair follicles, intestinal crypts and epidermis. Therefore, identifying drug targets that would result in the elimination of cancer cells, but not normal cells represents one of the top priorities in cancer research.

Despite significant advances in the development of targeted therapies, in the vast majority of cases, following an initial response, resistance rapidly emerges leading to recurrence and progression. We now understand that resistance emerges due to the heterogeneity including notably the fact that in most cancers, multiple oncogenes act simultaneously. As a result, inhibition of one oncogene can be overcome by another. Resistance also emerges due to mutations in cell death pathways notably anti-apoptotic mechanism.

Theoretically therefore, drugs able to 1- target cancer cells only while sparing highly proliferative but normal cells, 2- target a common denominator to multiple oncogenes rather than single oncogene and 3- activate multiple modes of cell death represent the ideal anti-cancer drug.

Large-scale screens aimed at identifying such ideal drugs have been conducted. Notably, the Varmus group conducted a high-throughput chemical screen which identified LCS-1 as such a molecule able to inhibit the growth of several different cancer cell lines[1]. They subsequently combined affinity proteomics and gene expression analyses to identify the target of LCS-1[2]. Their analysis revealed the unexpected observation that the copper/zinc dismutase SOD1 as the target of LCS-1[2]. Based on this finding, they tested the effect of the overexpression of SOD1 in a model of lung cancer cell lines and found that it promotes lung cancer cells growth, while reducing apoptosis[2]. In addition, Huang et al., also identified SOD1 as a target of an anti-cancer agent in leukemia[3].

SOD1 is an abundant enzyme required for the conversion of superoxide to hydrogen peroxide. Recent studies have shown that hydrogen peroxide acts as a signaling molecule to promote proliferation[4,5]. Therefore, SOD1 plays a dual role in reducing oxidative stress due to superoxide, as well as promoting signaling by increasing hydrogen peroxide. SOD1 localizes mainly to the cytoplasm but is also found in the nucleus and the inter-membrane space (IMS) of the mitochondria[6,7]. SOD1 has been mainly studied in amyotrophic lateral sclerosis (fALS), as it was the first gene found to be associated with familial form of the disease[8]. Therefore, the finding of SOD1 as a potential target in cancer therapy was not only surprising but also mechanistically puzzling.

Along with SOD1, the manganese dismutase SOD2 also converts superoxide to hydrogen peroxide, but unlike SOD1, SOD2 localization is restricted to the matrix of the mitochondria. However, SOD2 has been reported to be down-regulated in cancer[9,10] and the resulting elevation in ROS is reported to be associated with the stabilization of HIF1α and the switch to glycolysis[11].

Our group has a long-standing interest in the effect of ROS on the accumulation of misfolded protein in the mitochondria and the resulting activation of the mitochondrial unfolded protein response (UPR^{mt})[12–20]. Notably, we reported that the matrix sirtuin SIRT3 regulates one axis of the UPR^{mt} [13]. SIRT3 has several substrates in the matrix including the matrix dismutase SOD2[21,22]. In absence of SIRT3, SOD2 is inactive and as a result, ROS

production in the matrix increases. Our current model is that while SIRT3 and SOD2 decrease early during transformation, its reactivation later during tumorigenesis is associated with mitochondrial fitness and increased invasion[17]. In support of this notion, SOD2 was found to be elevated in metastases compared to primary breast cancer[17,23].

As SIRT3 is decreased in 87% of primary breast cancer[11], we hypothesized that the resulting increase in ROS may be counterbalanced by an up-regulation of SOD1, which would reduce ROS in the IMS but also in the cytoplasm and therefore contribute to an overall reduction of cellular ROS.

We reported that SOD1 is overexpressed in three independent mouse model of breast cancer including the MMTV-Wnt and MMTV-ErbB2 models[24] but whether SOD1 plays a role during transformation *in vivo* remained unknown. Therefore, in the current study, we used genetic crosses between the SOD1 knockout mice and the MMTV-inducible ErbB2 (iErbB2) and MMTV-Wnt mice to test the effect of SOD1 deletion on tumor formation *in vivo*. We also analyzed the effect of SOD1 genetic deletion on normal mammary gland development.

Our results indicate that SOD1 plays an essential house-keeping function during transformation in an oncogene-independent fashion. Further, our data suggest that deletion of SOD1 has no effect on normal mammary gland, skin or intestine and its absence during tumorigenesis leads to activation of both apoptosis and oncogene-induced senescence. This data supports the hypothesis that SOD1 may be essential for the adaptation of cancer cells to elevated oxidative stress due to superoxide and represents a very promising target.

Results

Oncogene-driven proliferation of mammary tumor fail to form in absence of SOD1

ErbB2 is a well-characterized oncogene in breast cancer[25,26]. ErbB2 expression in the mouse mammary gland using the mouse mammary tumor virus promoter (MMTV) either constitutively or using an inducible TET ON system (MMTV-iErbB2) has demonstrated its ability to promote aggressive tumor formation in mouse models[27–30]. We selected the inducible erbB2 (MMTV-iErbB2) model has it allows for the controlled and synchronized formation of mammary tumors with a frequency of more than 90% of mammary gland within 8 weeks of induction using 1.5 mg/kg of doxycycline in the drinking water[30]. The MMTV-iErbB2 mice were crossed to the SOD1 knockout mice to generate iErbB2 transgenic lines carrying the same genetic background but carrying either both copies of the SOD1 gene (SOD1+/+ iErbB2), heterozygotes carrying only one copy of the SOD1 gene (SOD1+/− iErbB2) or homozygotes lacking both copies of the SOD1 gene (SOD1−/− iErbB2). At 3 months of age, doxycycline was added to the drinking water of females of each genotype for six weeks.

After treatment, mice from all three genotypes were harvested. Analysis of the mammary glands of the SOD1+/+ iErbB2 females by whole mount revealed multifocal tumor formation of varying size (Fig. 1a, b, top panel) as well as hyper-proliferation along the ductal tree (Fig. 1a, b, top panel). Histological analysis of these foci confirmed that they represent adenocarcinoma of the mammary gland (Fig. 1c, top panel). As both tumor size

and the extent of hyper-proliferation showed some degree of variation, we established a scoring system whereby continuous hyper-proliferation along the ducts was scored as 3, dispersed hyper-proliferation was scored as 2 and ducts with morphology of normal mammary ducts were scored as 1 (Fig. 1d). Using this scoring system, we found that the mammary glands of the SOD1+/+ iErbB2 mice show 52% of ducts with a score of 3, 17% of ducts with a score of 2 and the remaining 31% ducts with a score of 1 (Fig. 1d). Tumor volume was also quantified using length and width of individual foci visualized by whole mount. This analysis revealed an average tumor volume of 1.01 mm^2 (Fig. 1e).

In the SOD1+/− iErbB2 heterozygote females, whole mounts revealed a reduction in both ductal proliferation and tumor volumes (Fig. 1a, b, c, middle panel). Upon quantification, we found that 32% of ducts had a score of 3, 22% a score of 2 and 46% of ducts a score of 1 (Fig. 1d). This reduction in ductal proliferation correlated with a decrease in tumor formation as the average tumor volume was 0.25 mm^2 (Fig. 1e).

In the SOD1−/− iErbB2 homozygote mice, tumor formation and hyper-proliferation were both drastically reduced (Fig. 1a, b, c, bottom panel). Quantification of the ductal proliferation showed that less the 7% of ducts with a score of 3 or 2 and the majority of 93% scored 1. This significant reduction in ductal proliferation correlated with an average tumor foci size of less than 0.13 mm^2 in volume (Fig. 1e). However, as smaller tumors remained detectable in absence of SOD1, we conducted deeper histological assessment of these residual tumors. We found that in contrast to the SOD1+/+ iErbB2 tumors which show high nuclear grade characteristic of aggressive tumors, the nuclear grade of residual SOD1−/− ErbB2 tumor was low indicating that these tumors are benign (Fig. 1f, g).

These results demonstrate that despite the very aggressive nature of the mammary tumor in the inducible ErbB2 mouse model, their formation is reduced in mice carrying only one copy of the SOD1 gene and abolished in absence of SOD1.

However, as doxycycline has been shown to affect mitochondrial translation[31] and SOD1 localizes partly to the mitochondria[6,7], to test for a potential indirect interaction between SOD1 and doxycycline and to also expand the analysis to other oncogenes, we also crossed the SOD1 knockout mice to the MMTV-Wnt transgenic mice. The Wnt oncogene is also a well-established mouse model of breast cancer[32]. Unlike the inducible erbB2 model, in the MMTV-Wnt model, the Wnt oncogene is constitutively expressed. In these mice, spontaneous tumors develop in 50% of older females but in young mice, the mammary glands are characterized by hyper-proliferation across the entire gland, which resemble the hyper-proliferation observed during pregnancy rather than distinct foci[33].

We generated three genetically matched colonies of SOD1+/+Wnt, SOD1+/− Wnt and SOD1−/− Wnt females and analyzed their mammary glands by whole mount at the age of 3 months. As expected, in the SOD1+/+ Wnt females displayed generalized ductal hyperplasia that mimics that observed during pregnancy (Fig. 2a, b, top panel). Histological analysis showed that at this time point, the hyper-proliferation was associated with dysplasia of the mammary duct and ductal filling resembling ductal carcinoma in situ (DCIS) (Fig. 2c). To quantify the hyperplasia, we established a scoring system whereby continuous hyperplasia

was scored as 3, dispersed hyperplasia was scored as 2 and no hyperplasia was scored as 1. Using this system, we found that 37% of the SOD1+/+ Wnt mammary gland ducts showing hyperplasia with a score of 3 and 57% with a score of 2 and less than 6% with a score of 1 (Fig. 2d).

In the SOD1+/− Wnt females, we observed mixed phenotype within the same mammary gland, where some area were hyper-proliferative while adjacent area were not (Fig. 2a, b, c, middle panel). Therefore, the overall quantification of the ductal hyperplasia resulted in a mild reduction in the percentage of ducts with a score of 3 to 28% and an increased in the percentage of duct with a score of 1 to 17% (Fig. 2 d).

In the SOD1−/− Wnt females however, the hyper-proliferation was severely reduced compare to the age-matched SOD1+/+ Wnt females (Fig. 2a, b, c, bottom panel). Quantification revealed that 17% of glands show a score of 3, 23% a score of 2 and 60% a score of 1 (Fig. 2c). In addition, the nuclear grade of residual DCIS-like lesion in the SOD1−/−/Wnt mice was significantly reduced (Fig. 2e).

Collectively, the analysis of the effect of gene dosage of SOD1 in both the inducible ErbB2 and the constitutive non-inducible Wnt model of mammary tumors led us to conclude that SOD1 is essential for tumor formation and its effect is oncogene-independent.

Depletion of SOD1 does not affect normal tissues hyper-proliferation.

The ductal hyper-proliferation observed in the Wnt model is reminiscent of the hyper-proliferation observed during pregnancy. As depletion of SOD1 abolished the proliferation in the Wnt model, this observation raised the possibility that SOD1 may also be required for the non-oncogenic ductal hyper-proliferative normally observed during pregnancy. This concern is also supported by the report that SOD1 is selectively increased in the luminal cells of the mammary gland[34]. Therefore, to address this possibility, we analyzed the mammary glands of SOD1+/+, SOD1+/− and SOD1−/− females during pregnancy in absence of oncogene. Females were mated and their mammary glands harvested for analysis by whole mount following pregnancy. As expected the mammary gland of SOD1+/+ females showed hyper-proliferation (Fig. 3a, b, c, top panel). In the SOD1+/− and SOD1−/− females, we found no significant difference in either ductal hyper-proliferation (Fig. 3a, b, c, middle and bottom panels). This observation is consistent with the fact, SOD1−/− mothers are able to lactate and generate viable litters demonstrating that the function of the mammary gland during pregnancy is intact in these mice[35,36].

Therefore, this result indicates that while SOD1 is essential to maintain hyper-proliferation driven by the ErbB2 or Wnt oncogene, it is dispensable for the non-oncogenic hyper-proliferation associated with pregnancy.

Post-natal invasion of the fat pad represents another phase of mammary gland development that is characterized by increased proliferation. We therefore monitored the effect of SOD1 on fat pad invasion during puberty. In the SOD1+/+ and SOD1+/− females no significant difference between the rate of invasion or number of terminal end buds (TEB) were found (Fig. 3 d, e, f, top and middle panels). In the SOD1−/− females however a significant delay

in the rate of fat pad invasion and number of TEB was found (Fig. 3 d, e, f, bottom panels). However, this delay ultimately did not affect mammary gland development as no significant differences in the morphology of the mammary gland in virgin adult females were observed between the three genotypes (Fig. 3g, h, i).

To further test the potential effect of SOD1 inhibition on highly proliferative tissues, the skin and intestinal crypts were also analyzed. In mice of 3 months of age, we found no significant differences between the three genotypes (Fig. 3 j, k).

Overall, these results show that lack of SOD1 has limited to no effect on normal mammary gland development, does not affect pregnancy-associated proliferation or other hyper-proliferative tissues such as the skin and intestine.

Oncogene activation promotes increase in superoxide levels and SOD1 expression.

Having established that SOD1 is essential for oncogene-mediated proliferation but not cellular proliferation associated with normal mammary gland development, we next aimed at defining the mechanism of this specificity. As SOD1 function is to convert superoxide to hydrogen peroxide, we reasoned that the specificity of the effect of SOD1 in oncogene-driven proliferation might be related to alteration in superoxide levels upon oncogene activation. To test this possibility, we used isolated primary mammary epithelial cells (MEC) from the MMTV-iErbB2 females. To expand these cells ex vivo, we adapted a recent protocol developed for the expansion of human of primary breast epithelial cells expansion *ex vivo*[37]. Using this protocol, primary mammary epithelial cells from the MMTV-iErbB2 mice were expanded *ex vivo* in absence of doxycycline for 24 hours. We then induced ErbB2 for 72 hours using doxycycline and measured the level of ROS in both un-induced and induced cells. We found in the un-induced ErbB2 MECs, 24% of cells show elevated superoxide levels (Fig. 4a, higher panel). However, upon induction of ErbB2 for only 24 hours, the percentage of cells with elevated superoxide raised to 36% (Fig. 4a, lower panel). This result supports previous findings that activation of oncogenes promotes an elevation in ROS[38,39]. To test if the elevation in superoxide is linked to the differential effect of SOD1 in oncogene-induced versus pregnancy-induced hyper-proliferation, we repeated the analysis in MECs from virgin or pregnant females. We found a slight increase in some mice (Fig. 4b) but a decrease in others resulting in no statistical significant difference in the levels of superoxide (Fig. 4c) between MECs from virgin or pregnant females.

As we found that ErbB2-activation increases superoxide, we then tested if induction of ErbB2 also increases SOD1 *in vivo*. To test this possibility, we induced ErbB2 using doxycycline for 3 months in order to promote the formation of large palpable tumors (Fig. 4d). The primary tumors and the adjacent mammary glands were harvested and stained for SOD1 levels by immunohistochemistry. We found that within the same sections where ducts that look histologically normal and primary tumors are found, that the normal ducts are negative for SOD1 staining while the primary tumors express SOD1 at high levels (Fig. 4e). Quantification of the staining revealed that mild SOD1 positivity, scored as 2, could be observed in ducts showing early dysplasia but strong SOD1 staining scored as 3 was only observed in tumors (Fig. 4f). However, SOD1 was not elevated in the hyper-proliferative ducts during pregnancy (Fig. 4g).

To complement the analysis of superoxide of primary ErbB2 MECs, we sorted ErbB2 cells directly from fully established primary tumors. We found that the fraction of cells with elevated superoxide increases drastically in primary tumors (Fig. 4h). We then performed western analysis of SOD1 in low and high superoxide sub-populations from the same ErbB2 primary tumors and found that the high superoxide sub-population across all mice shows elevation in SOD1 levels (Fig. 4i, j).

Therefore, these results indicate that the specificity of SOD1 for oncogene-mediated proliferation correlates with the elevation in superoxide levels in cancer cells, which is not observed in highly proliferative normal cells.

Depletion of SOD1 leads to activation of apoptosis and senescence.

In lung cancer cell lines, inhibition of SOD1 using either LCS-1 or ATN-224 leads to apoptosis[1,2,40]. In the latter study, ATN224 was shown to decrease in the anti-apoptotic protein MCL1[40]. To test whether the genetic ablation of SOD1 also induces cell death through a decrease in MCL1, we monitored MCL1 in the mammary gland of the SOD1+/+ ErbB2, SOD1+/− ErbB2 and SOD1−/− ErbB2 females. Surprisingly, we found no evidence of a decrease in MCL-1 in the mammary glands between the three genotypes. In contrast, we found an increase in the short form of MCL-1 (MCL-1s), which is pro-apoptotic (Fig. 5a, b)[41]. We reasoned that in contrast to established cell lines used in the previous studies, in our model, the oncogene is induced in normal mammary epithelial cells. As oncogene activation promotes oncogene-induced senescence[42,43], we tested whether senescence may contribute to the inhibition of growth observed in the mammary glands in our models. Using p53 and p16 as markers of senescence, we found a significant increase in both markers in the SOD1−/−ErbB2 mammary glands (Fig. 5a, b). To confirm that senescence was induced in the epithelial cells, we performed immunohistochemistry of p16 and found a significant increase in p16 in the SOD1−/−/ErbB2 mammary glands (Fig. 5c, d).

As mammary gland extracts contain several cell types in the stroma in addition to the mammary ducts, we next aimed at isolating primary MECs from all three genotypes for further analyses. However, we found that SOD1 null cells do not grow under standard *in vitro* conditions, suggesting that these cells are already under elevated stress conditions and are unable to adapt to growth on plastic.

We therefore pursued the analysis in 3D culture by plating cells on matrigel. Under these conditions only the SOD1+/+ ErbB2 and SOD1+/− ErbB2 MECs survived *ex vivo*. We performed a time course following addition of doxycycline to the media to induce ErbB2 in MEC. Under these conditions, we found that induction of ErbB2, in presence of both copies of SOD1 gene, led to rapid growth of organoids (Fig. 5e, f) characterized by intruding morphology (Fig. 5g). However, the induction of ErbB2 in cells carrying only one copy of SOD1 did not promote the growth of organoids and the small colonies retained a rounded morphology (Fig. 5e, f, g). The same organoids were used for staining with MCL-1, which recognizes both the long and short form of the protein. We found staining for MCL-1 only in the heterozygote MECs (Fig. 5h). Since these cells failed to grow (Fig. 5e) and the mammary glands *in vivo* show elevation of the pro-apoptotic MCL-1s, we interpret this staining as representing MCL1s. We also used these organoids for staining with beta-

galactosidase, another standard marker of senescence that cannot be used by western or on paraffin sections. We found an increase in beta-gal staining in the SOD1+/−/ErbB2 cells (Fig. 5i, j).

Our data indicate that deletion of SOD1 results in reduction of tumor initiation. To test the effect pharmacological inhibition of SOD1 on established mammary tumors, we tested the effect of the SOD1 inhibitor LCS-1 on ErbB2 tumor cells. For this experiment, we took advantage of our inducible ErbB2 tumor bank in which ErbB2 expression is induced in mice until large palpable tumors are formed. Tumors were then harvested and frozen. These ErbB2 cancer cells were seeded on matrigel and allowed to form colonies in presence of doxycycline to maintain expression. We found that treatment with the SOD1 inhibitor LCS1 drastically inhibited colony formation (Fig. 5k, l) and cellular proliferation (Fig. 5m). These results are consistent with previous reports of the induction of apoptosis in established cancer cell lines following treatment with SOD1 inhibitors[2,3,40,44].

Collectively, therefore our results indicate that deletion of SOD1 severely reduces the ability of oncogene-driven tumor formation and this is linked to the induction of both apoptosis and oncogene-induced senescence.

Elevated SOD1 is associated with poor survival and increased metastasis in all sub-type of breast cancer.

In order to validate our findings in humans, we interrogated the Gene Expression Omnibus dataset using KM plotter[45] to determine whether elevated expression of SOD1 is associated with clinical outcome in breast cancer. We found that primary breast cancers with elevated SOD1 levels are associated with highly significant lower relapse free survival (Fig. 6a), overall survival (Fig. 6b) and metastasis free survival (Fig. 6c). However, we found that SOD1 expression is not restricted or enriched in any breast cancer sub-type and elevated expression of SOD1 correlates lower survival in all sub-types (Fig. 6e, f, g). These findings are in agreement with the notion that SOD1 carries a housekeeping function that is shared by all breast cancer sub-types and is independent of the oncogenes driving the growth of these tumors.

Discussion

Oxidative stress plays a role in both signaling and cell death depending on their levels[4,10]. SOD1 and SOD2 are the main enzymes against oxidative stress, yet SOD2 has been reported to be decreased at least in the initial phase of cancer formation and allow the switch to glycolysis[9–11]. We previously suggested that a SOD2 to SOD1 switch maybe necessary to counterbalance the elevation in superoxide due to the decrease in SOD2[24,46]. However, if correct this hypothesis implies that SOD1 may play an essential role in tumor initiation. Here, we provide genetic evidences supporting this hypothesis. We demonstrate that SOD1 is essential for tumor formation by crossing the SOD1 knockout mice with two independent models of breast cancer. We also demonstrate that the effect of SOD1 is independent of the oncogene-driving tumor formation and in humans, SOD1 is found in all breast cancer sub-types. This is consistent with the observation that the SOD1 inhibitor LCS1 was effective in killing a wide number of cancer cell lines from specific cancer types but also from various

cancer types[1,24,47]. This finding is significant as it suggests that SOD1 maybe a universal target by affecting a housekeeping function rather than a specific oncogenic driver.

In addition, the current study demonstrates that the inhibition of SOD1 does not affect normal cells with increased proliferation. This finding is also significant as toxicity of most anti-cancer drugs is due to their ability to target any cells that are actively proliferating. Our results suggest that the specificity of SOD1 for cancer cells is due to the increase in superoxide associated with oncogene activation, which is not observed in normal cells. We further show that in primary mammary tumors, the high superoxide sub-population of cells shows an elevation in SOD1 compared to the low superoxide sub-population. Based on these observations, we propose that under baseline level of superoxide, SOD1 is dispensable however, when levels of superoxide reach higher levels, cancer cells up-regulate SOD1 as to lower superoxide levels under a threshold that is compatible with maintenance of cellular integrity and survival. (Fig. 7a). We propose that the elevation in superoxide upon oncogenic activation represents a therapeutic window of SOD1 inhibitors, as failure to limit the elevation in superoxide leads to activation of apoptosis and oncogene-induced senescence (Fig. 7a).

Our finding that SOD1 is essential for tumor initiation integrates well with the recent report that mTORC1 regulates SOD1 through phosphorylation[48]. In this study, the authors describe that under starvation conditions, mTORC1 is inactivated and as a result, SOD1 is up-regulated[48]. They reported that the elevation in SOD1 under starvation conditions is necessary to enhance cancer cell survival and contribute to chemo-resistance[48]. Therefore, since early lesions do not have established vascularization and are under starvation conditions, the effect of starvation on SOD1 may well represent the mechanism by which SOD1 is up-regulated early during transformation (Fig. 7b).

We found that genetic deletion of SOD1 leads to induction of apoptosis as well as oncogene-induced senescence. Since inhibition of SOD1 is predicted to increase superoxide and decrease hydrogen peroxide levels, two potential mechanisms to explain these observations were possible: cell death due to increase superoxide or inhibition of the signaling mediated by hydrogen peroxide[49]. However, we found no evidence of a decrease in hydrogen peroxide in mammary epithelial cells of SOD1 −/−ErbB2 mice (Suppl. Fig.1). This result is in agreement with the surprising elevation of hydrogen peroxide in lung cancer cells treated with SOD1 inhibitor ATN-224[40]. While in our model we observed a similar trend toward an elevation in hydrogen peroxide, it did not reach statistical significance. This result nevertheless argues that inhibition of signaling is not the predominant mechanism by which inhibition of SOD1 reduces tumor formation.

The results presented in the current study also clarify further the timing of the SOD2 to SOD1 switch we previously proposed[24]. Collectively, the down-regulation of SOD2[9,11,24] and the elevation on SOD1[2,24,46] coincide only with the early stage of transformation (Fig. 7b). SOD2 is exclusively in the matrix of the mitochondria, while SOD1 is in both the cytoplasm and the inter-membrane space of the mitochondria. We previously shown that in cancer cells, the mitochondrial fraction of SOD1 increases[24]. Therefore, we propose that the effect of SOD1 is in monitoring the levels of superoxide in the cytoplasm but importantly

also in the mitochondria especially when SOD2 levels are low. This interpretation is consistent with the observation that treatment with the inhibitor of SOD1, LCS-1, leads to mitochondrial morphological abnormalities that are not observed in normal cells under the same conditions[24]. SOD2 has been reported to be up-regulated later during transformation and to be associated late disease stages[50]. This finding is in line with our work indicating a link between SOD2 expression and the invasive capacity of breast cancer cells[17].

Therefore, as long term use of SOD1 inhibitors in the prevention setting in humans is an unlikely option, we propose that the results presented in the current study predict that SOD1 inhibitors may be of particular use in early stage breast cancer such as DCIS and be less effective in metastatic disease where other defense mechanisms against oxidative stress, such as up-regulation of SOD2 may take place. These possibilities will need to be tested in the future.

Materials and Methods

Animal Experiments

SOD1 knockout (B6.129S7-Sod1^{tm1Leb}/DnJ) mice were purchased from Jackson Laboratory. The mice were crossed with MMTV-rtTA/TetO-NeuNT (iErbB2) (kindly provided by Lewis Chodosh) or MMTV-Wnt (B6SJL-Tg(Wnt1)1Hev/J) (Jackson Laboratory) mice to generate SOD1 wild-type (+/+), SOD1 heterozygous (+/−) and SOD1 (−/−) knockout in the respective transgenic background. Genotyping was performed by polymerase chain reaction using DNA extracted from tail using the following primers: SOD1 (5’-TGTTCTCCTCTTCCTCATCTCC-3’; 5’-ACCCTTTCCAAATCCTCAGC-3’, 5’-TGAACCAGTTGTGTTGTCAGG-3’, 5’-TCCATCACTGGTCACTAGCC-3’), rtTA (5’-TGCCGCCATTATTACGACAAGC-3’; 5’-ACCGTACTCGTCAATTCCAAGGG-3’), ErBb2 (5’-TTTCCTGCAGCAGCCTACGC-3’, 5’-CGGAACCCACATCAGGCC-3’), Wnt (5’-GGACTTGCTTCTCTTCTCATAGCC-3’, 5’-CCACACAGGCATAGAGTGTCTGC-3’, 5’-CAAATGTTGCTTGTCTGGTG-3’, 5’-GTCAGTCGAGTGCACAGTTT-3’).

All mice used in experiments were 12 weeks old, unless otherwise described. For the SOD1-iErbB2 tumorigenesis analysis, SOD1 +/+ iErbB2 (n=5), SOD1 +/− iErbB2 (n=5), and SOD1 −/− iErbB2 (n=5) mice were given 1.5 g/L doxycycline in the drinking water every 5 days for 6 weeks. For the SOD1-MMTV-Wnt hyper-proliferation analysis, SOD1 +/+ Wnt (n=9), SOD1 +/− Wnt (n=9), and SOD1 −/− Wnt (n=5) mice were harvested at 15–20 weeks of age. For the mammary gland development studies, mice were harvested at indicated time points (for pregnancy SOD1 +/+ (n=5), SOD1 +/− (n=5), and SOD1 −/− (n=5) mice; for postnatal SOD1 +/+ (n=3), SOD1 +/− (n=3), and SOD1 −/− (n=4) mice, for adult SOD1 +/+ (n=5), SOD1 +/− (n=5), and SOD1 −/− (n=4) mice, for skin and intestine analysis SOD1 +/+ (n=4), SOD1 +/− (n=4), and SOD1 −/− (n=4) mice. For superoxide level analysis of virgin (n=6) and pregnant (n=4) mammary glands, pregnant females were checked for vaginal plugs and harvested at day 14. For the analysis SOD1 expression and reactive oxygen species in tumors, iErbB2 mice (n=4) were given 1.5 g/L doxycycline in the drinking water every 5 days for 3 months. Mice were euthanized and mammary glands were collected and either flash frozen, formalin fixed, or mounted on slides for whole mount analysis. All

experiments were approved by the Institutional Animal Care and Use Committee of the Icahn School of Medicine at Mount Sinai.

Whole Mount Analysis

Mouse abdominal mammary glands were mounted on glass slides and fixed in Carnoy's fixative (ethanol:chloroform:glacial acetic acid, 6:3:1) overnight. Glands were then stained in carmine aluminum stain overnight according to standard protocol. Whole mounts were imaged using a Zeiss Stemi 300 macroscope.

Mouse Mammary Tissue Isolation

Mouse mammary glands were excised from SOD1-iErbB2 mice, diced, and digested in a trypsin/collagenase mix for 25 minutes shaking at 37°C. Mammary epithelial tissues were retrieved by centrifuging for 5 minutes at 1000 rpm. The tissue was washed twice with Dulbecco's modified Eagle's medium/Nutrient Mixture F-12 (DMEM/F12) (Gibco, Carlsbad, CA, USA) and incubated with 2 U/μL DNase for 5 minutes at room temperature. The mammary organoids were isolated by pulse spinning twice at 1000 rpm. The pellet was then used for either three-dimensional or two-dimensional culture.

Primary Cell Culture

Primary cell lines derived from SOD1-iErbB2 mammary glands were grown in DMEM / F12 (1:1) supplemented with 5% Fetal Bovine Serum (FBS), 100 U/mlL Penicillin/ Streptomycin (P/S) (Gibco), 25 ng/mL Hydrocortisone (Sigma Aldrich, Saint Louis, MO), 2 μg/mL Amphotericin B (Gibco), and 2 μg/mL Doxycycline hyclate (Sigma Aldrich). Cells were grown in 5% CO_2 at 37°C.

Three-dimensional culturing of mammary organoids was performed as follows. An initial layer of growth factor reduced matrigel (Corning, Bedford, MA) was first allowed to solidify for 30 minutes in the incubator. Mammary organoids were resuspended in 5% matrigel and plated on the supporting layer. After 30 minutes, mammary epithelial cell (MEC) media (DMEM/F12, 1% insulin, transferrin, selenium, and 1% penicillin/streptomycin) with 2 μg/mL doxycycline was added. Media was changed every two days. Experiments were performed five times per time point. Brightfield images were captured using a Leica DMI300 inverted microscope.

Immunohistochemistry (IHC)

Formalin-fixed tissue was processed and paraffin embedded by the Biorepository Core Facility at Mount Sinai. Slides were sectioned, mounted, and stained for hematoxylin and eosin by the core facility. Unstained slides were deparaffinized with xylene and rehydrated with decreasing ethanol gradients. Antigen retrieval was performed in citrate buffer pH 6.0 at 95°C for 30 minutes. Sections were treated with Dual Endogenous Enzyme Block (DAKO, Glostrup, Denmark) for 15 minutes and then incubated with Normal Antibody Diluent (MP Biomedicals, Solon, OH, USA) for 1 hour at room temperature. Primary antibody staining for p16 (Santa Cruz, Santa Cruz, CA, USA, sc-1661) was performed at 4°C overnight at a dilution of 1:50. Primary antibody staining for SOD1 (Santa Cruz, Santa Cruz, CA, USA, sc-11407) was performed at room temperature for 2 hours at a dilution of

1:100. Secondary antibody staining was performed with Biotinylated Anti-mouse (Jackson ImmunoResearch, West Grove, PA, USA, 115-065-205) or Biotinylated Anti-rabbit (Jackson ImmunoResearch, West Grove, PA, USA, 711-065-152) at room temperature for 1 hour. Slides were incubated with Streptavidin-HRP (Vector Laboratories, Burlingame, CA, USA, SA-5004) for 30 minutes. Washes were carried out with Tris Buffered Saline with 0.04% Tween. Antigen detection was performed using aminoethyl carbazole (AEC) peroxidase substrate kit (Vector Laboratories, SK-4200). Counterstaining was performed with hematoxylin. Sections were washed with water and mounted with Vectamount aqueous mounting media (Vector Laboratories, H-5501). Images were captured using a Zeiss AX10 microscope.

Flow Cytometry and Fluorescence Associated Cell Sorting (FACS)

After tissue isolation, mammary epithelial cells (MEC) were washed with phosphate buffered saline (PBS) and passed through a 70μm single cell strainer. Cells were resuspended in Hanks Balanced Salt Solution (HBSS) with 0.5% Bovine Serum Album (BSA) and incubated with 5 μM MitoSOX Red (ThermoFisher, Rockford, IL, USA, M36008) or 5 μM CM-H2DCFDA (ThermoFisher, C6827) for 30 minutes at 37°C. Cells were washed twice and passed through a single cell strainer again before flow cytometry or FACS. BD FACSDiva software was used to excite and capture the populations of interest. Flow cytometry was performed on a BD Canto and FACS was performed on a BD FACSAria II.

Western Blotting

Flash frozen mammary glands were pulverized and lysed using NP40 lysis buffer with protease inhibitors (1 g/ml leupeptin, 1 g/ml pepstatin, 100 g/ml phenylmethylsulfonyl fluoride). Samples were sonicated for 1 second at 20% amplitude twice, centrifuged at 14,000 rpm for 5 minutes at 4°C to remove the fatty layer followed by centrifugation at 14,000 rpm for 15 minutes at 4°C. Protein lysate concentrations were determined using a Bradford Assay. Protein lysates were run on a SDS-PAGE electrophoresis gel and transferred to nitrocellulose membrane (GE Healthcare, Buckinghamshire, UK). The membrane was blocked using 5% non-fat dry milk and then probed using the appropriate primary antibodies: MCL-1 (1:500, Santa Cruz, sc-20679), p53 (1:2000, EMB Millipore, San Diego, CA, USA, OP33), p16 (1:500, Santa Cruz, sc-1661), actin (1:10,000, EMB MiIlipore, MAB1501). Secondary antibody incubation was performed with either horseradish peroxidase conjugated anti-mouse or anti-rabbit antibodies (KwikQuant, Greenwich, CT, USA). Chemiluminescence was detected using the KwikQuant system.

Immunofluorescence

Mammary organoids were fixed with 4% paraformaldehyde at room temperature for 10 minutes. The organoids were washed twice with PBS, incubated with methanol for 2 minutes, followed by a 2 minutes incubation in PBS with 1% Triton-X. The organoids were permeabilized by incubating with penetration buffer (0.2% Triton-X, 0.3M glycine, 20% DMSO in PBS) for 15 minutes. Samples were then blocked with blocking buffer (5% mouse serum, 5% rabbit serum, 5% goat serum, 2% bovine serum albumin, 0.5% Triton X, 10% DMSO in PBS). MCL-1 (1:100, Santa Cruz, sc-20679) primary antibody was diluted in

antibody buffer (50% blocking buffer, 0.2% Tween-20) and samples were incubated for 1 hour at room temperature on a shaker. Secondary antibody incubation with goat anti-mouse Alexa Fluor 488 (ThermoFisher A-11001) conjugated antibodies at a dilution of 1:200 was performed in the dark at room temperature for 1 hour. Samples were then washed five times before mounting on a slide using PBS:glycerol (1:1). Images were captured using a Leica SP3 confocal microscope. Images were pseudo-colored using ImageJ.

Beta-galactosidase staining

Cells were washed with PBS pH 5.5, then fixed with 0.5% glutaraldehyde in PBS for 15 minutes. Cells were then incubated with β-galactosidase substrate (1 mg/mL 5-bromo-4-chloro-3-inolyl-β-D-galactoside (β-gal), 5 mM potassium ferrocyanide, 5 mM potassium ferricyanide, 1mM MgCl2 in PBS at pH 5.5) at 37°C for 3 hours. Cells were then washed twice with water and analyzed under light microscopy.

Colony Formation Assay

Primary cell lines were derived from mammary tumors of iErbB2 mice induced with 1.5g/L doxycycline for 3 months. Primary cells were grown in DMEM / F12 (1:1) supplemented with 10% Fetal Bovine Serum (FBS), 100 U/mlL Penicillin/Streptomycin (P/S) (Gibco), 25 ng/mL Hydrocortisone (Sigma Aldrich, Saint Louis, MO), 2 μg/mL Amphotericin B (Gibco), and 2 μg/mL Doxycycline hyclate (Sigma Aldrich). Single cells were resuspended in 5% matrigel and plated on the supporting layer or matrigel. Cells were treated with either dimethyl sufoxide (Sigma Aldrich) or 3 μM LCS-1 (EMB Millipore, San Diego, CA, USA, 567417). Experiments were performed in triplicate. Images were captured at 3X magnification using a Zeiss Stemi 300 macroscope.

MTT Proliferation Assay

Primary mouse mammary tumor cells were grown in DMEM / F12 (1:1) supplemented with 10% Fetal Bovine Serum (FBS), 100 U/mlL Penicillin/Streptomycin (P/S) (Gibco), 25 ng/mL Hydrocortisone (Sigma Aldrich, Saint Louis, MO), 2 μg/mL Amphotericin B (Gibco), and 2 μg/mL Doxycycline hyclate (Sigma Aldrich). Cells were treated with either DMSO (Control) or 3 μM LCS-1 (EMB Millipore) for 24 hours. Cells were incubated with MTT ((3-(4,5-Dimethylthiazol-2-yl)-2,5-Diphenyltetrazolium Bromide) (Sigma) at 0.5 mg/mL for three hours. Experiments were performed in triplicate. Absorbance was measured at 570nM.

Bioinformatic Analyses

Kaplan Meier plots were generated using KM Plotter (Győrffy et al., 2010; Lánczky et al., 2016, http://kmplot.com/) using the SOD1 probe (200642_at). Patients were stratified into high and low SOD1 expression groups by using the auto select best cutoff option.

Statistics

Statistical analyses were performed using GraphPad Prism Software. Statistical tests performed are included in figure legends. The p value cutoff was set to 0.05. ns = not

significant, * $p < 0.05$, ** $p < 0.01$, *** $p < 0.001$, **** $p < 0.0001$. Data were displayed as mean ± standard error of the mean (SEM).

Supplementary Material

Refer to Web version on PubMed Central for supplementary material.

Acknowledgments:

We would like to thank all members of the Germain lab and of the Mount Sinai Flow Cytometry Core, Microscopy Core and Biorepository Core Facility. This study was supported by the NIH R01CA172046 to D.G and the NIH supplement to M.G. The core facilities used in this study are supported by P30 grant CA196521.

References

1. Somwar R, Shum D, Djaballah H, Varmus H. Identification and Preliminary Characterization of Novel Small Molecules That Inhibit Growth of Human Lung Adenocarcinoma Cells. J Biomol Screen 2009; 14: 1176–1184. [PubMed: 19887599]
2. Somwar R, Erdjument-Bromage H, Larsson E, Shum D, Lockwood WW, Yang G et al. Superoxide dismutase 1 (SOD1) is a target for a small molecule identified in a screen for inhibitors of the growth of lung adenocarcinoma cell lines. Proc Natl Acad Sci 2011; 108: 16375–16380. [PubMed: 21930909]
3. Huang P, Feng L, Oldham EA, Keating MJ, Plunkett W. Superoxide dismutase as a target for the selective killing of cancer cells. Nature 2000; 407: 390–395. [PubMed: 11014196]
4. Schieber M, Chandel NS. ROS function in redox signaling and oxidative stress. Curr. Biol 2014; 24: 453–462.
5. Pelicano H, Xu RH, Du M, Feng L, Sasaki R, Carew JS et al. Mitochondrial respiration defects in cancer cells cause activation of Akt survival pathway through a redox-mediated mechanism. J Cell Biol 2006. doi:10.1083/jcb.200512100.
6. Okado-Matsumoto A, Fridovich I. Subcellular distribution of superoxide dismutases (SOD) in rat liver. Cu,Zn-SOD in mitochondria. J Biol Chem 2001; 276: 38388–38393. [PubMed: 11507097]
7. Sturtz LA, Diekert K, Jensen LT, Lill R, Culotta VC. A Fraction of Yeast Cu,Zn-Superoxide Dismutase and Its Metallochaperone, CCS, Localize to the Intermembrane Space of Mitochondria. J Biol Chem 2001; 276: 38084–38089. [PubMed: 11500508]
8. Rosen DR, Siddique T, Patterson D, Figlewicz DA, Sapp P, Hentati A et al. Mutations in Cu/Zn superoxide dismutase gene are associated with familial amyotrophic lateral sclerosis. Nature 1993; 362: 59–62. [PubMed: 8446170]
9. Oberley LW, Buettner GR. Role of superoxide dismutase in cancer: a review. Cancer Res 1979; 39: 1141–9. [PubMed: 217531]
10. Wang Y, Branicky R, Noë A, Hekimi S. Superoxide dismutases: Dual roles in controlling ROS damage and regulating ROS signaling. J Cell Biol 2018; 217: jcb.201708007.
11. Finley LWS, Carracedo A, Lee J, Souza A, Egia A, Zhang J et al. SIRT3 Opposes Reprogramming of Cancer Cell Metabolism through HIF1α Destabilization. Cancer Cell 2011; 19: 416–428. [PubMed: 21397863]
12. Papa L, Germain D. Estrogen receptor mediate a distinct mitochondrial unfolded protein response. JCS 2011;: 1396–1402.
13. Papa L, Germain D. SirT3 regulates the mitochondrial unfolded protein response. Mol Cell Biol 2014. doi:10.1128/MCB.01337-13.
14. Kenny TC, Germain D. From discovery of the CHOP axis and targeting ClpP to the identification of additional axes of the UPRmt driven by the estrogen receptor and SIRT3. J Bioenerg Biomembr 2017; 49: 297–305. [PubMed: 28799020]
15. Kenny TC, Germain D. mtDNA, Metastasis, and the Mitochondrial Unfolded Protein Response (UPRmt). Front Cell Dev Biol 2017; 5: 37. [PubMed: 28470001]

16. Kenny TC, Manfredi G, Germain D. The Mitochondrial Unfolded Protein Response as a Non-Oncogene Addiction to Support Adaptation to Stress during Transformation in Cancer and Beyond. Front Oncol 2017; 7: 159. [PubMed: 28798902]
17. Kenny TC, Hart P, Ragazzi M, Sersinghe M, Chipuk J, Sagar M et al. Selected mitochondrial DNA landscapes activate the SIRT3 axis of the UPR mt to promote metastasis. Oncogene 2017; 36: 4393–4404. [PubMed: 28368421]
18. He C, Hart PC, Germain D, Bonini MG. SOD2 and the Mitochondrial UPR: Partners Regulating Cellular Phenotypic Transitions. Trends Biochem. Sci 2016; 41: 568–577. [PubMed: 27180143]
19. Riar AK, Burstein SR, Palomo GM, Arreguin A, Manfredi G, Germain D. Sex specific activation of the ERα axis of the mitochondrial UPR (UPRmt) in the G93A-SOD1 mouse model of familial ALS. Hum Mol Genet 2017; 26: 1318–1327. [PubMed: 28186560]
20. Germain D Toward the identification and the targeting of key players of the mitochondrial unfolded protein response (UPRmt) in cancer. J Bioenerg Biomembr 2017; 49: 291.
21. Tao R, Coleman MC, Pennington JD, Ozden O, Park SH, Jiang H et al. Sirt3-Mediated Deacetylation of Evolutionarily Conserved Lysine 122 Regulates MnSOD Activity in Response to Stress. Mol Cell 2010; 40: 893–904. [PubMed: 21172655]
22. Lombard DB, Tishkoff DX, Bao J. Mitochondrial sirtuins in the regulation of mitochondrial activity and metabolic adaptation. Handb Exp Pharmacol 2011; 206: 163–188. [PubMed: 21879450]
23. Hempel N, Carrico PM, Melendez JA. Manganese superoxide dismutase (Sod2) and redox-control of signaling events that drive metastasis. Anticancer Agents Med Chem 2011; 11: 191–201. [PubMed: 21434856]
24. Papa L, Hahn M, Marsh EL, Evans BS, Germain D. SOD2 to SOD1 switch in breast cancer. J Biol Chem 2014; 289: 5412–5416. [PubMed: 24448804]
25. Slamon DJ, Godolphin Will, Jones LA, Holt JA, Wong SG, Keith DE et al. Studies of the HER-2 / neu Proto-Oncogene in Human Breast and Ovarian Cancer. Science (80-) 1989; 244: 707–712.
26. Elster N, Collins DM, Toomey S, Crown J, Eustace AJ, Hennessy BT. HER2-family signalling mechanisms, clinical implications and targeting in breast cancer. Breast Cancer Res. Treat 2015; 149: 5–15. [PubMed: 25542271]
27. Bouchard L, Lamarre L, Tremblay PJ, Jolicoeur P. Stochastic appearance of mammary tumors in transgenic mice carrying the MMTV/c-neu oncogene. Cell 1989; 57: 931–936. [PubMed: 2567634]
28. Muller WJ, Sinn E, Pattengale PK, Wallace R, Leder P. Single-step induction of mammary adenocarcinoma in transgenic mice bearing the activated c-neu oncogene. Cell 1988; 54: 105–115. [PubMed: 2898299]
29. Guy CT, Webster MA, Schaller M, Parsons TJ, Cardiff RD, Muller WJ. Expression of the neu protooncogene in the mammary epithelium of transgenic mice induces metastatic disease. Proc Natl Acad Sci 1992; 89: 10578–10582. [PubMed: 1359541]
30. Moody SE, Sarkisian CJ, Hahn KT, Gunther EJ, Pickup S, Dugan KD et al. Conditional activation of Neu in the mammary epithelium of transgenic mice results in reversible pulmonary metastasis. Cancer Cell 2002; 2: 451–461. [PubMed: 12498714]
31. Moullan N, Mouchiroud L, Wang X, Ryu D, Williams EG, Mottis A et al. Tetracyclines disturb mitochondrial function across eukaryotic models: A call for caution in biomedical research. Cell Rep 2015; 10: 1681–1691. [PubMed: 25772356]
32. Li Y, Hively WP, Varmus HE. Use of MMTV-Wnt-1 transgenic mice for studying the genetic basis of breast cancer. Oncogene 2000; 19: 1002–1009. [PubMed: 10713683]
33. Tsukamoto AS, Grosschedl R, Guzman RC, Parslow T, Varmus HE. Expression of the int-1 gene in transgenic mice is associated with mammary gland hyperplasia and adenocarcinomas in male and female mice. Cell 1988; 55: 619–625. [PubMed: 3180222]
34. Kannan N, Nguyen LV, Makarem M, Dong Y, Shih K, Eirew P et al. Glutathione-dependent and -independent oxidative stress-control mechanisms distinguish normal human mammary epithelial cell subsets. Proc Natl Acad Sci 2014; 111: 7789–7794. [PubMed: 24821780]
35. Matzuk MM, Dionne L, Guo Q, Kumar TR, Lebovitz R. Ovarian function in superoxide dismutase 1 and 2 knockout mice. Endocrinology 1998; 139: 4008–4011. [PubMed: 9724058]

36. Ho YS, Gargano M, Cao J, Bronson RT, Heimler I, Hutz RJ. Reduced fertility in female mice lacking copper-zinc superoxide dismutase. J Biol Chem 1998; 273: 7765–7769. [PubMed: 9516486]
37. Palechor-Ceron N, Suprynowicz FA, Upadhyay G, Dakic A, Minas T, Simic V et al. Radiation Induces Diffusible Feeder Cell Factor(s) That Cooperate with ROCK Inhibitor to Conditionally Reprogram and Immortalize Epithelial Cells. Am J Pathol 2013; 183: 1862–1870. [PubMed: 24096078]
38. Weinberg F, Hamanaka R, Wheaton WW, Weinberg S, Joseph J, Lopez M et al. Mitochondrial metabolism and ROS generation are essential for Kras-mediated tumorigenicity. Proc Natl Acad Sci 2010; 107: 8788–8793. [PubMed: 20421486]
39. Sabharwal SS, Schumacker PT. Mitochondrial ROS in cancer: Initiators, amplifiers or an Achilles' heel? Nat. Rev. Cancer 2014; 14: 709–721. [PubMed: 25342630]
40. Glasauer A, Sena LA, Diebold LP, Mazar AP, Chandel NS. Targeting SOD1 reduces experimental non-small-cell lung cancer. J Clin Invest 2014; 124: 117–128. [PubMed: 24292713]
41. Bae J, Leo CP, Hsu Y, Hsueh AJW. MCL-1S, a Splicing Variant of the Antiapoptotic BCL-2 Family Member MCL-1, Encodes a Proapoptotic Protein Possessing Only the BH3 Domain* 2000. doi:10.1074/jbc.M909826199.
42. Serrano M, Lin AW, McCurrach ME, Beach D, Lowe SW. Oncogenic ras provokes premature cell senescence associated with accumulation of p53 and p16(INK4a). Cell 1997; 88: 593–602. [PubMed: 9054499]
43. Sarkisian CJ, Keister BA, Stairs DB, Boxer RB, Moody SE, Chodosh LA. Dose-dependent oncogene-induced senescence in vivo and its evasion during mammary tumorigenesis. Nat Cell Biol 2007; 9: 493. [PubMed: 17450133]
44. Li S, Fu L, Tian T, Deng L, Li H, Xia W et al. Disrupting SOD1 activity inhibits cell growth and enhances lipid accumulation in nasopharyngeal carcinoma. Cell Commun Signal 2018; 16: 28. [PubMed: 29891006]
45. Győrffy B, Lanczky A, Eklund AC, Denkert C, Budczies J, Li Q et al. An online survival analysis tool to rapidly assess the effect of 22,277 genes on breast cancer prognosis using microarray data of 1,809 patients. Breast Cancer Res. Treat 2010; 123: 725–731. [PubMed: 20020197]
46. Papa L, Manfredi G, Germain D. SOD1, an unexpected novel target for cancer therapy. Genes Cancer 2014; 5: 15–21. [PubMed: 24955214]
47. Sajesh BV, McManus KJ, Babu V. Sajesh KJM. Targeting SOD1 induces synthetic lethal killing in BLM- and CHEK2-deficient colorectal cancer cells. Oncotarget 2015; 6: 27907–27922. [PubMed: 26318585]
48. Tsang CK, Chen M, Cheng X, White E, Burley SK, Steven XF et al. SOD1 Phosphorylation by mTORC1 Couples Nutrient Sensing and Redox Regulation Article SOD1 Phosphorylation by mTORC1 Couples Nutrient Sensing and Redox Regulation. Mol Cell 2018; 70: 502–515.e8. [PubMed: 29727620]
49. Reddi AR, Culotta VC. SOD1 Integrates Signals from Oxygen and Glucose to Repress Respiration. Cell 2013; 152: 224–235. [PubMed: 23332757]
50. Hart PC, Mao M, Luelsdorf A, De Abreu P, Ansenberger-Fricano K, Ekoue DN et al. ARTICLE MnSOD upregulation sustains the Warburg effect via mitochondrial ROS and AMPK-dependent signalling in cancer. Nat Commun 2015; 6. doi:10.1038/ncomms7053.

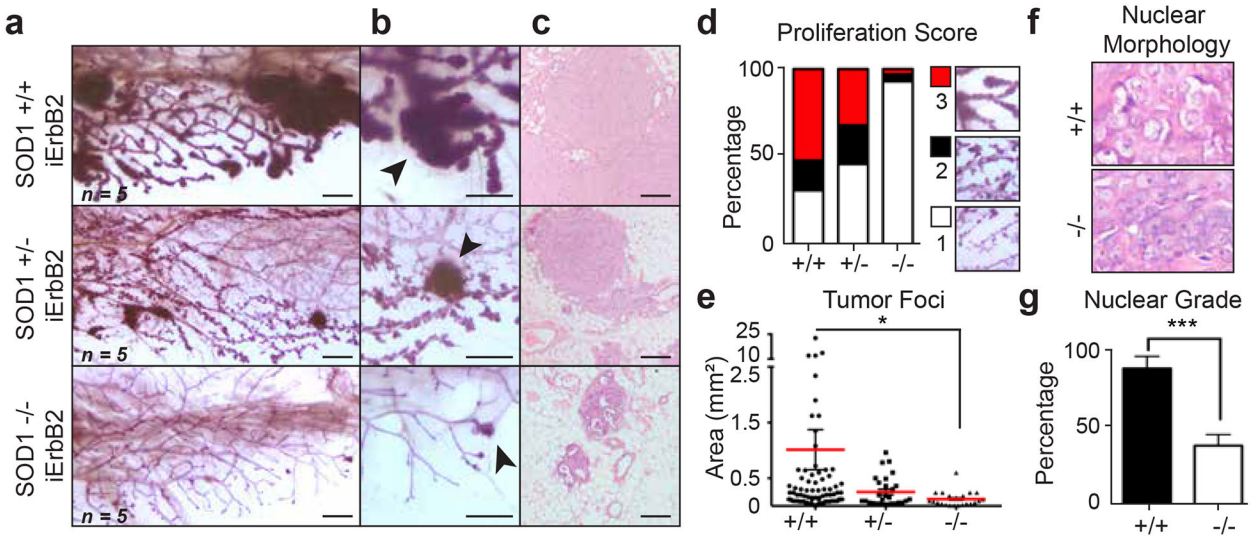

Figure 1. Absence of SOD1 inhibits tumor proliferation and growth in iErbB2 driven mammary tumors.

(a and **b)** Whole mount analysis of SOD1 wildtype (+/+, n=5), SOD1 heterozygous (+/−, n=5), and SOD1 null (−/−, n=5) iErbB2 mice after 6 weeks of induction with doxycycline. Scale bar represents 1 mm. Arrow shows tumor lesion. Images were taken at 0.8X (a) or 2X (b) magnification.

(c) Representative paraffin sections of mammary glands stained with hematoxylin and eosin at 5X magnification. Scale bar represents 100 μm.

(d) Proliferation along the mammary duct was quantified from low to high using 1 (low), 2 (moderate) 3 (high) scale. Representative images of scoring shown on far right.

(e) Tumor lesions in the mammary glands of SOD1 +/+, SOD1 +/−, and SOD1 −/− iErbB2 mice. Tumor lesions size were recorded by measuring the length and width. SOD1 +/+ iErbB2 (mean = 1.01 ±0.36 mm2, n=85), SOD1 +/− iErbB2 (mean = 0.25 ±0.05 mm2, n=28), and SOD1 −/− iErbB2 (mean = 0.13 ±0.03 mm2, n=22). Data were analyzed using a Kruskal-Wallis test. Error bars represent ± SEM. * $p < 0.05$

(f) Representative image of nuclear morphology of SOD1 +/+ and SOD1 −/− tumors. Images taken at 40X magnification.

(g) Quantification of high nuclear grade morphology in SOD1 +/+ and SOD1 −/− tumors. Data were analyzed using a Student's t test. Error bars represent ± SEM. *** $p < 0.0005$.

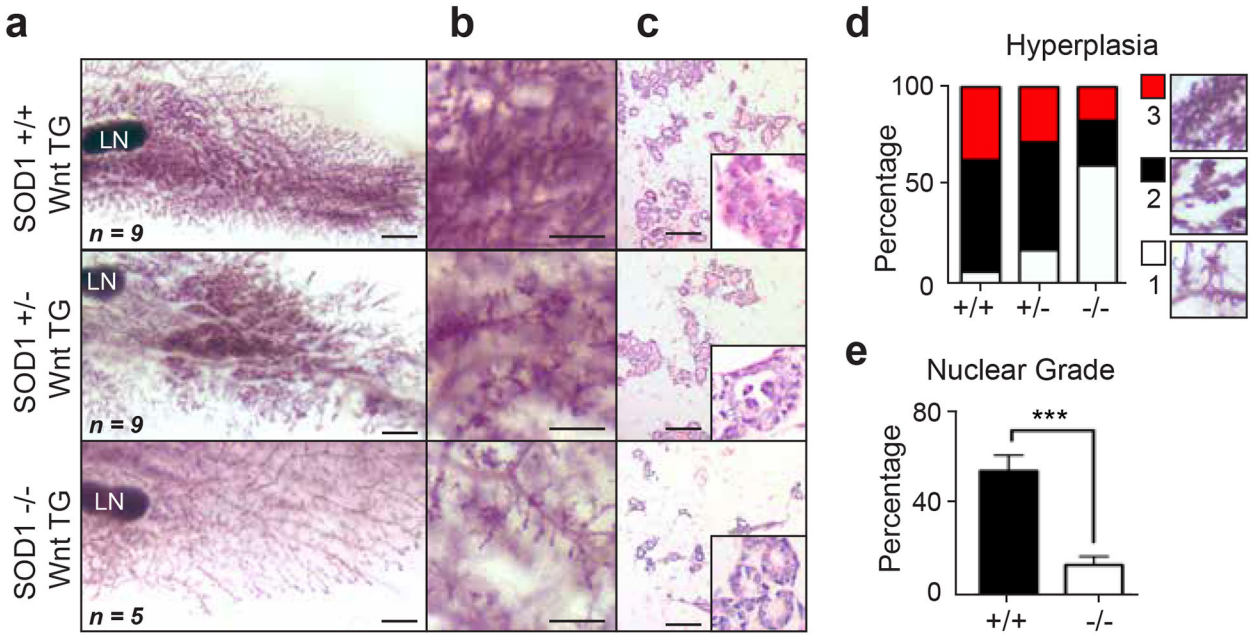

Figure 2. Absence of SOD1 inhibits hyperproliferation in Wnt driven mammary tumors.

(a and **b)** Whole mount analysis of SOD1 wildtype (+/+, n=9), SOD1 hemiyzgous (+/−, n=9), and SOD1 null (−/−, n=5) Wnt mice at 12 weeks of age. Scale bar represents 1 mm. Images were taken at 0.8X (a) or 2X (b) magnification.

(c) Representative paraffin sections of mammary glands stained with hematoxylin and eosin at 10X magnification. Scale bar represents 100 μm.

(d) Hyperplasia was quantified from low to high using 1(low), 2(moderate), 3 (high) scale on three representative mice per genotype. Representative images of scoring shown on far right.

(e) Quantification of high nuclear grade morphology in SOD1 +/+ and SOD1 −/− Wnt lesions. Data was analyzed using Student's t test. Error bars represent ± SEM. *** $p < 0.0005$.

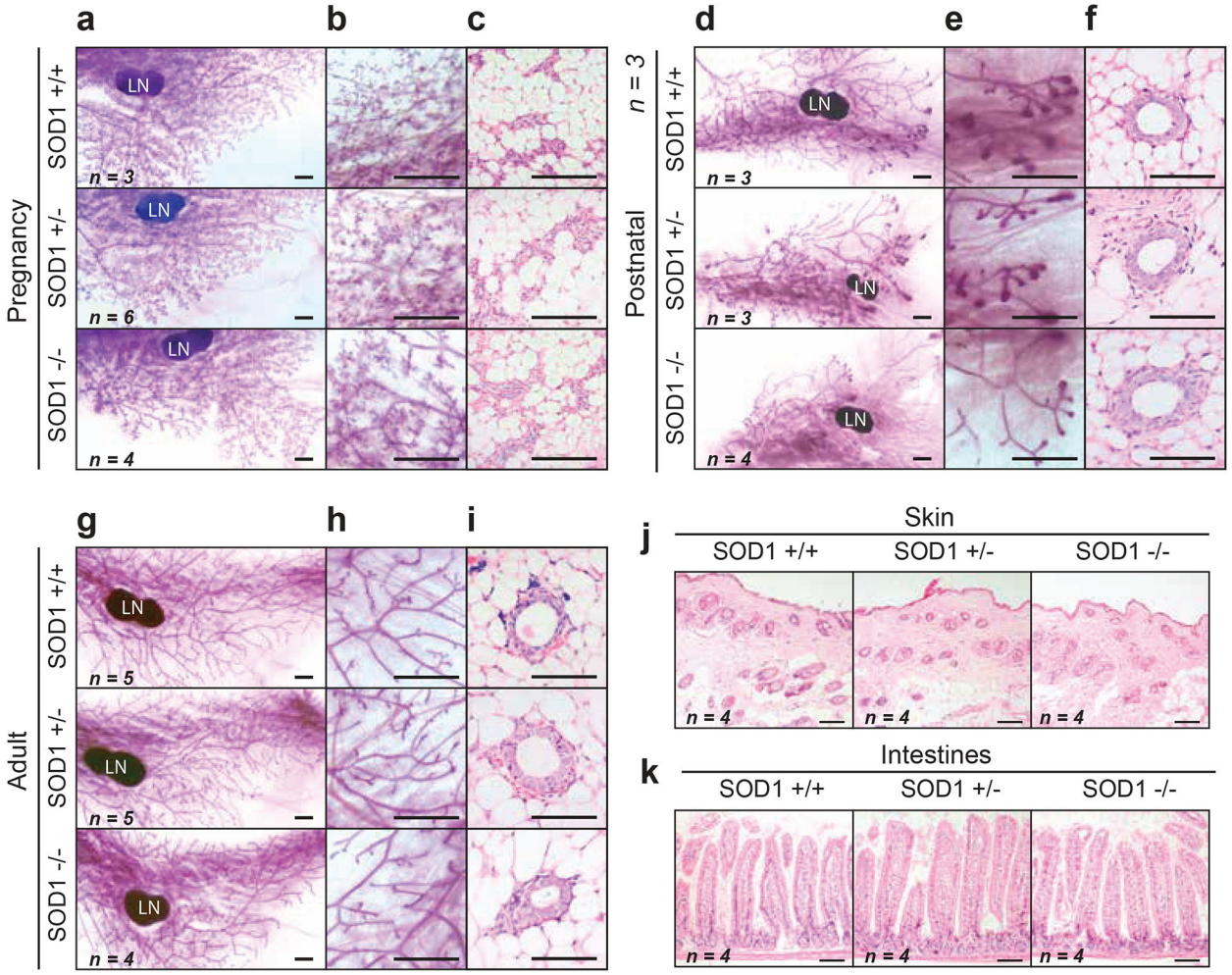

Figure 3. SOD1 is not necessary for normal proliferation.

(a and **b)** Whole mount analysis of SOD1 wildtype (+/+, n=3), SOD1 heterozygous (+/−, n=6), and SOD1 null (−/−, n=4) mice after pregnancy. Scale bar represents 1 mm. Images were taken at 0.8X (a) or 2X (b) magnification.

(c) Representative paraffin sections of mammary ducts stained with hematoxylin and eosin at 20X magnification. Scale bar represents 100 μm.

(d and **e)** Whole mount analysis of SOD1 +/+ (n=3), SOD1 +/− (n=3), and SOD1 −/− (n=4) mice 4 weeks after birth. Scale bar represents 1 mm. Images were taken at 0.8X (a) or 2X (b) magnification.

(f) Representative paraffin sections of mammary ducts stained with hematoxylin and eosin at 40X magnification. Scale bar represents 100 μm.

(g and **h)** Whole mount analysis of SOD1 +/+ (n=5), SOD1 +/− (n=5), and SOD1 −/− (n=4) adult mice at 3 months. Images taken under 0.8X (a) or 2X (b) objective.

(i) Representative paraffin sections of mammary ducts stained with hematoxylin and eosin at 40X magnification. Scale bar represents 100 μm.

(j) Representative paraffin sections of epidermis from SOD1 +/+ (n=4), SOD1 +/− (n=4), and SOD1 −/− (n=4) mice stained with hematoxylin and eosin at 40X magnification. Scale bar represents 100 μm.

(k) Representative paraffin sections of intestines from SOD1 +/+ (n=4), SOD1 +/− (n=4), and SOD1 −/− (n=4) stained with hematoxylin and eosin at 40X magnification. Scale bar represents 100 μm.

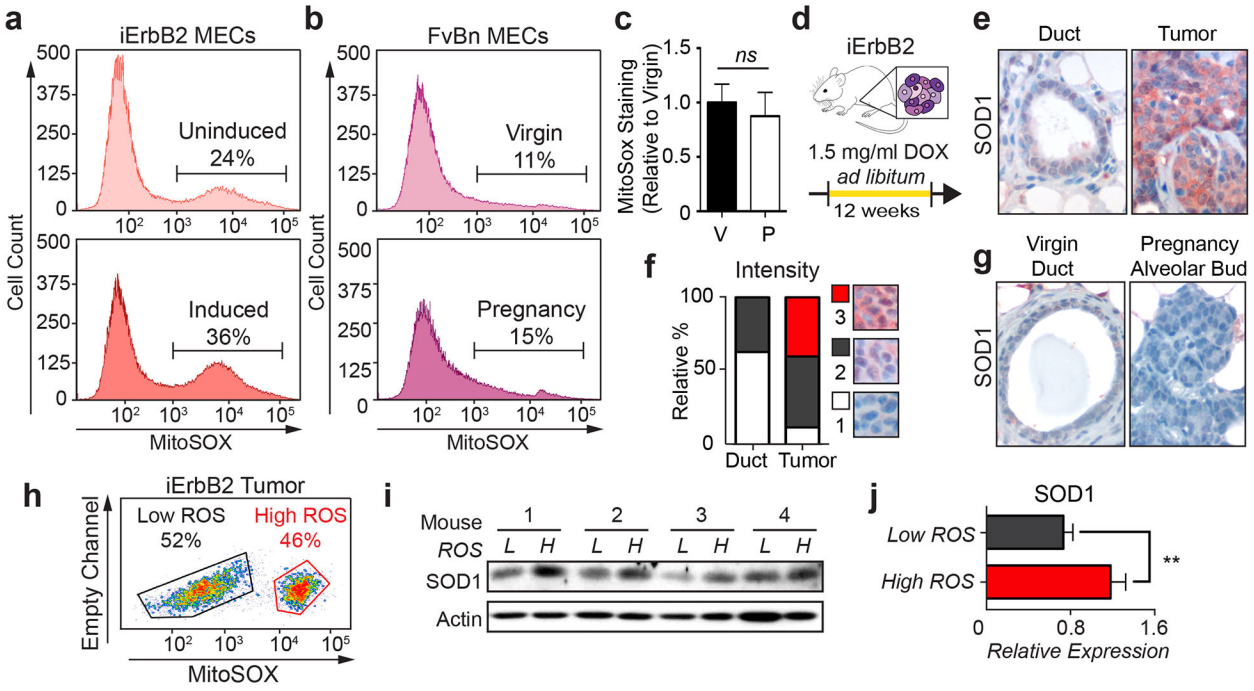

Figure 4. SOD1 is necessary to cope with oxidative stress during transformation.

(a and **b)** Flow cytometry of superoxide levels as measured by MitoSOX in mammary epithelial cells from iErbB2 mice un-induced or induced with doxycycline and (b) mammary epithelial cells from virgin or pregnant female mice.

(c) Quantification of superoxide levels in mammary glands from virgin (n=6) versus pregnant mice (n=4).

(d) Schematic of experimental design. Mice were induced with doxycycline in drinking water *ad libitum* for 3 months (n=4).

(e) Representative SOD1 immunohistochemistry of virgin mammary duct and pregnant mammary alveolar bud.

(f) Quantification of SOD1 staining using scoring scale 1+ (low), 2+ (moderate), 3+ (high). Representative images of scoring shown on far right.

(g) Representative SOD1 immunohistochemistry of normal mammary duct and iErbB2 mammary tumor.

(h) Representative dot plot of flow cytometry associated sorting (FACS) of mammary tumors from iErbB2 mice. Cells were gated low or high superoxide levels as measured by MitoSOX staining.

(i) Immunoblot of SOD1 in sorted tumor cells with low (L) or high (H) superoxide.

(j) Quantification of SOD1 expression from (g) relative to actin.

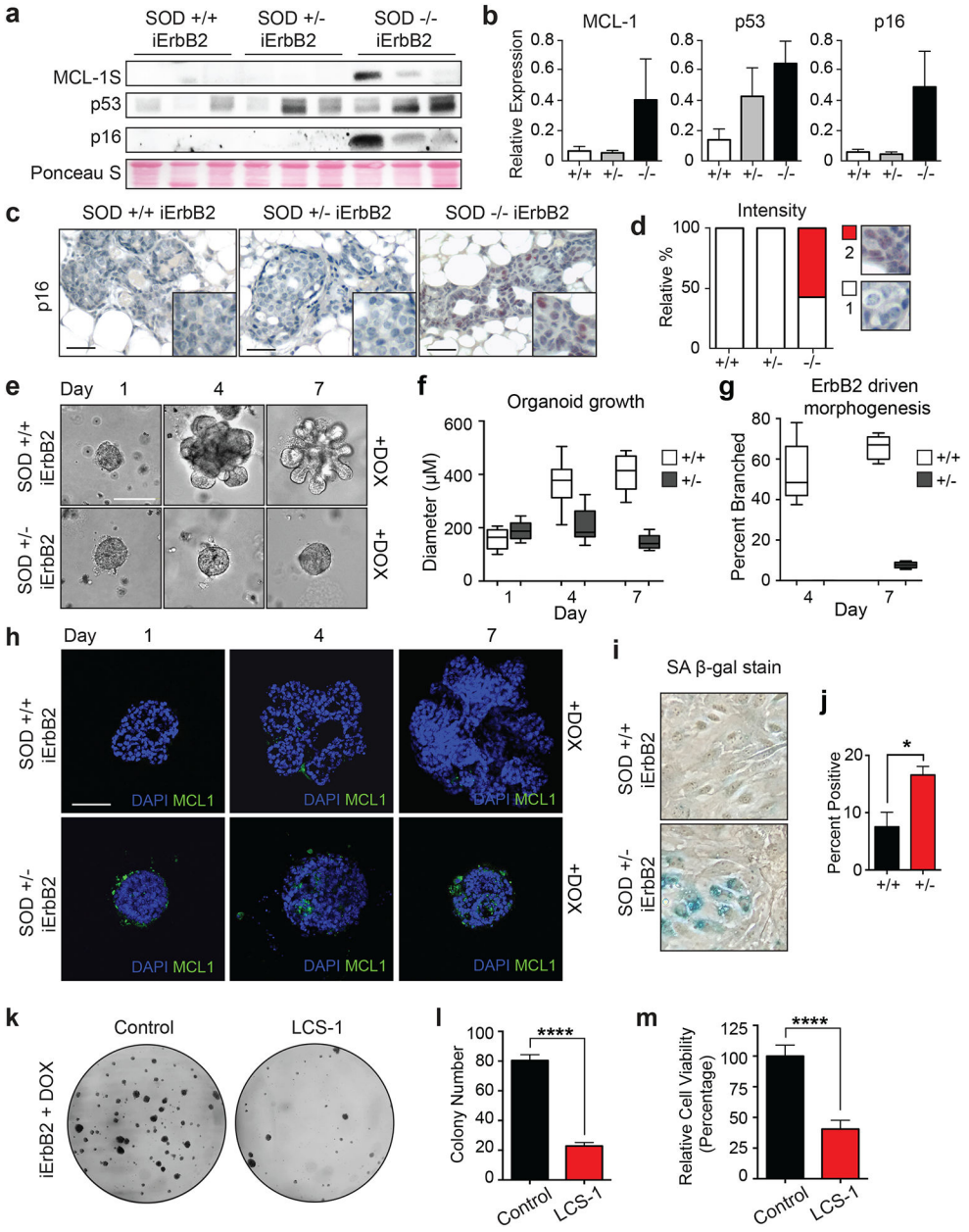

Figure 5. SOD1 is necessary for oncogene-driven proliferation of primary mouse epithelial cells.

(a) Immunoblotting of MCL1-s, p53, and p16 of SOD1 +/+, SOD1 +/−, and SOD1 −/− iErBb2 mammary gland.

(b) Quantification of MCL1-s, p53, and p16 expression from (a) relative to loading.

(c) Representative images of immunohistochemistry of p16 in SOD +/+, SOD +/−, and SOD −/− iErbB2 mammary glands.

(d) Quantification of percentage of positive p16 stain from (c).

(e) Brightfield images of 3D primary mammary epithelial organoids from SOD +/+ and SOD +/− iErbB2 mice in the presence doxycycline at Day 1 (n=5), 4 (n=5), and 7 (n=5). Scale bar represents 100 uM.

(f) Measurements of diameter of 3D organoids from (e).

(g) Percentage of organoids from (e) with ErbB2 driven morphogenesis (n=3, 10 observations per time point).

(h) Immunofluorescence of MCL-1 (green) in SOD +/+ and SOD +/− erbB2 organoids. Nuclei were stained with DAPI.

(i) Representative images of Senescence-Associated-β-galactosidase (SA-β-gal) staining of SOD +/+ and SOD +/− iErbB2 mammary epithelial cells.

(j) Percentage of SA-β-gal positive cells.

(k) Representative images of colony formation assay or iErb2 tumor cells treated with DMSO (Control) or SOD1 inhibitor LCS-1 (n = 5).

(l) Quantification of colony formation assay in k.

(m) MTT Proliferation assay of iErb2 tumor cells treated with DMSO (Control) or LCS-1 (n = 3).

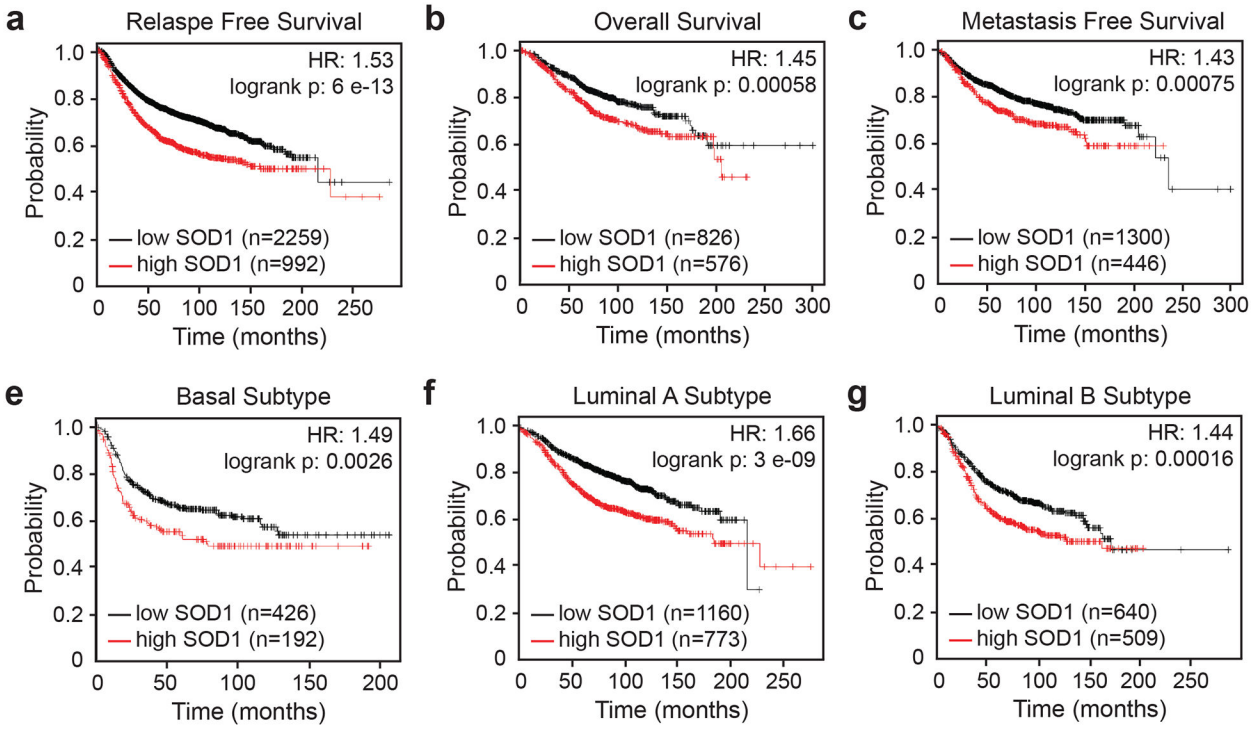

Figure 6. High SOD1 expression correlates with poorer prognosis in breast cancer patients.

(a) Kaplan Meier analysis of relapse free survival in breast cancer patients (n=3251) with low or high SOD1 expression. HR = hazard ratio.

(b) Kaplan Meier analysis of overall survival in breast cancer patients (n=1402) with low or high SOD1 expression.

(c) Kaplan Meier analysis of metastasis survival in breast cancer patients (n=1746) with low or high SOD1 expression.

(d) Kaplan Meier analysis of relapse free survival in basal breast cancer patients (n=618) with low or high SOD1 expression.

(e) Kaplan Meier analysis of relapse free survival in luminal A breast cancer patients (n=1933) with low or high SOD1 expression.

(f) Kaplan Meier analysis of relapse free survival in luminal B breast cancer patients (n=1149) with low or high SOD1 expression.

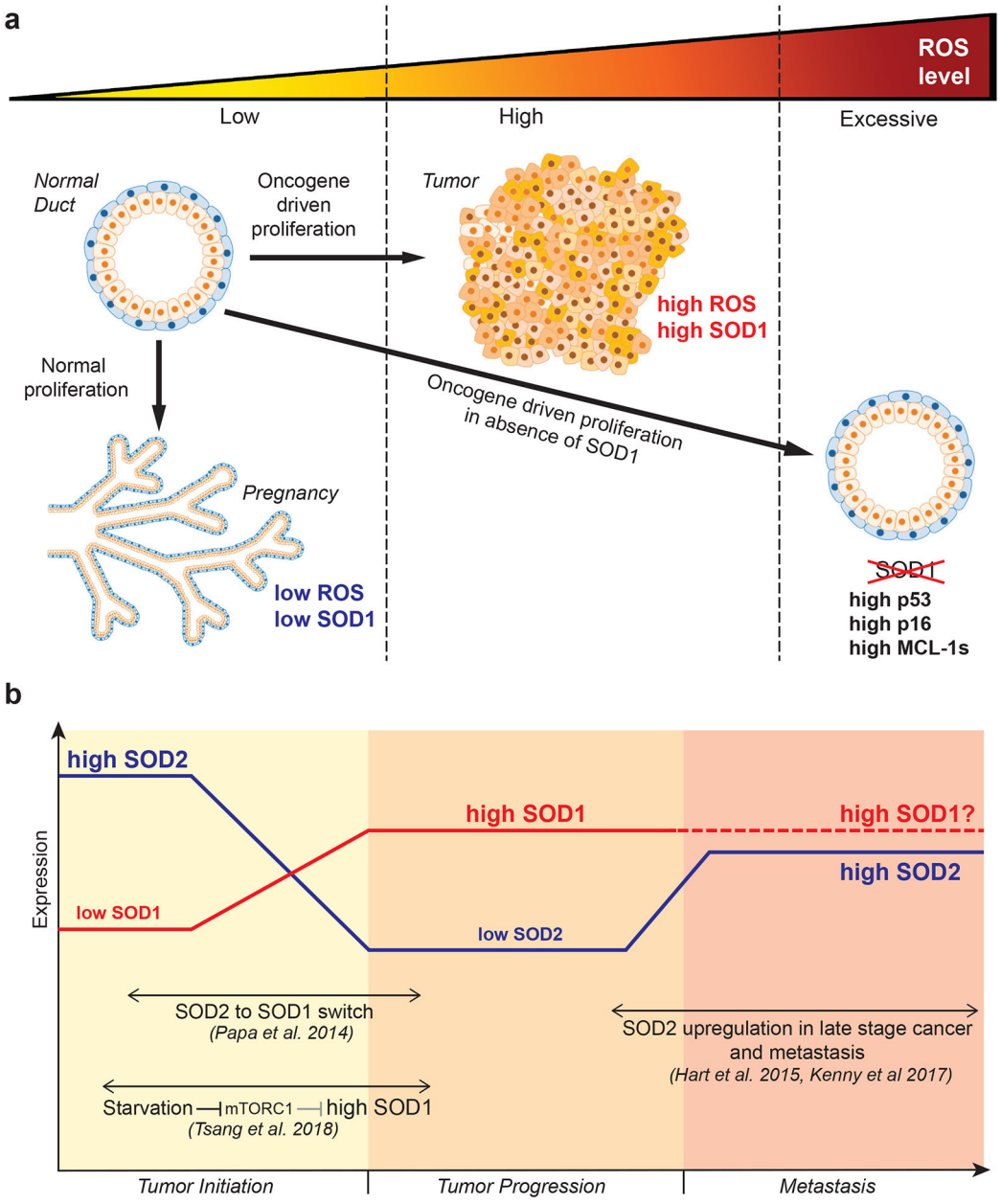

Figure 7. Model of the requirement of SOD1 either in response to oxidative stress in oncogene-driven during transformation or normal proliferation in the mammary gland.

a) In normal mammary ducts, the levels of ROS are low and remain low despite normal cellular proliferation as observed during pregnancy (left side). During oncogene-driven proliferation however, ROS increases (middle). Our results suggest that under these conditions, SOD1 also increases and prevents ROS levels from reaching excessive levels. In absence of SOD1 (right side), ROS reach excessive levels leading to apoptosis, oncogene-induced senescence and prevent proliferation.

b) Model of how the increase in SOD1 integrates with the changes in SOD2 over breast cancer progression from initiation to metastasis. The references are listed below the indicated changes in either SOD1 or SOD2.